

# Calculation and validation of material tests with specimens made out of filled elastomers

Philipp Thumann<sup>1</sup>, Krzysztof Swidergal<sup>1</sup>, Marcus Wagner<sup>1</sup>

<sup>1</sup> Ostbayerische Technische Hochschule Regensburg  
Department of Mechanical Engineering  
Laboratory for FEM (Finite-Element-Method)

## Abstract

In deep-drawing dies for steel sheet parts of car bodies huge masses are moved. To prevent vibrations, which occur by sudden acceleration or stopping of those masses, elastomeric tubular dampers [1] are used. The dampers are made out of carbon filled elastomers. A good knowledge about the material behaviour of metals is available. But for the numerical investigation of complete deep-drawing dies the elastomeric dampers must be taken into account, too. To characterize the material behaviour of the elastomers tensile tests and pressure tests were carried out. The received material data from the tests were read into LS-DYNA [2]. Simulation models of the tensile test and the pressure test were created for LS-DYNA according to the real dimensions and boundary conditions. For validation purposes, calculations of loading cycles were done to enable a comparison between test data and simulation results. For the calculations the implemented material model **\*MAT\_SIMPLIFIED\_RUBBER\_WITH\_DAMAGE (\*MAT\_183)** was used. The comparison shows a good fitting between the test data and the calculation results with respect to the mechanical material behaviour by using this material model in single loading cases. The settings from the simulations of material tests were transferred to simulations of dampers, which are used in deep-drawing dies.

## 1 Introduction

Nowadays, more and more manufacturing processes are being simulated by engineers. In automotive industry one of these processes is the forming of car bodies, which are made out of steel sheets. The car bodies are formed by using deep-drawing dies. A wide range of knowledge in numerical calculation of metal parts is available. But in deep-drawing dies also other materials are used, e.g. elastomers. There are many open questions regarding elastomer parts because of the complex behaviour of this material. In LS-DYNA several material models for rubberlike materials are available. In the investigation described below the material model **\*MAT\_SIMPLIFIED\_RUBBER\_WITH\_DAMAGE (\*MAT\_183)** is used. **\*MAT\_183** requires input data to reproduce the elastomeric behaviour. Therefore, it is possible to read in tables, which describe the stress-strain relations. These stress-strain relations were determined by tensile and pressure tests. In this paper the simulations of the material tests and a real rubber part (damper) by using **\*MAT\_183** are explained. Furthermore, the comparison and validation of the simulations are described below in detail.

## 2 Theory

Elastomers show a highly non-linear stress-strain relation. It is not sufficient to describe the material behaviour with the Young's modulus  $E$  and the Poisson's ratio  $\nu$ . Rather, so-called hyperelastic material models are used in FE analyses. With the help of the strain energy density function  $W$  the relation between stress and strain can be described with equation (1)

$$\sigma_i = \frac{\partial W}{\partial \lambda_i} . \quad (1)$$

Here the stretch ratio  $\lambda$  stands for the ratio between final length  $L$  and the length at the beginning  $L_0$  according to equation (2)

$$\lambda = \frac{L}{L_0} . \quad (2)$$

The stretch ratio  $\lambda$  can also be described with the nominal engineering strain  $\varepsilon$

$$\lambda = \frac{L_0 + \Delta L}{L_0} = 1 + \frac{\Delta L}{L_0} = 1 + \varepsilon , \quad (3)$$

see [3]. To characterize the strain energy density function  $W$  there are several polynomial approaches available, e.g. the Ogden model, see equation (4)

$$W = \sum_{i=1}^N \frac{2\mu_i}{\alpha_i^2} (\lambda_1^{\alpha_i} + \lambda_2^{\alpha_i} + \lambda_3^{\alpha_i} - 3), \quad (4)$$

see [4]. In the rubber model **\*MAT\_SIMPLIFIED\_RUBBER\_WITH\_DAMAGE** a modified Ogden model is used. That material model is contained within the LS-DYNA material library. In the following it is called **\*MAT\_183** according to the internal identification number and it is described in detail below.

## 2.1 LS-DYNA \*MAT\_183

Instead of the basic equation (4) in **\*MAT\_183** a modified form is used, see equation (5)

$$W = \sum_{n=1}^3 \sum_{i=1}^N \frac{\mu_i}{\alpha_i} (\lambda_n^{\alpha_i} - 1) + K(III_V - 1 - \ln III_V). \quad (5)$$

This equation contains an additional term for compressibility.  $K$  specifies the bulk modulus,  $\lambda_n^* = \lambda_n \cdot III_V^{-1/3}$  and  $III_V = \lambda_1 \cdot \lambda_2 \cdot \lambda_3$ . Furthermore  $\mu_i$  and  $\alpha_i$  are material constants.

Through equation (6) one can then consider the general constitutive relationship for hyperelasticity

$$\sigma_i = \frac{1}{\lambda_j \lambda_k} \frac{\partial W}{\partial \lambda_i}. \quad (6)$$

Equation (6) is the general hyperelastic constitutive relationship that relates principal stress to principal stretch. The indices  $i, j$ , and  $k$  are used to indicate Eigenvalues, where  $i, j$  and  $k$  each represent a different eigenvalue 1, 2 or 3. Substituting equation (5) into equation (6), we find the Ogden hyperelastic constitutive law according to equation (7)

$$\sigma_i = \sum_{i=1}^N \frac{\mu_i}{III_V} \left[ \lambda_n^{\alpha_i} - \sum_{n=1}^3 \frac{\lambda_n^{\alpha_i}}{3} \right] + K \frac{III_V - 1}{III_V}. \quad (7)$$

**\*MAT\_183** uses an equivalent form from equation (7) that eliminates the experimental constants in the expression. Equation (8) results in

$$\sigma_i = \frac{1}{III_V} \left[ f_0(\lambda_i) - \frac{1}{3} \sum_{n=1}^3 f_0(\lambda_n) \right] + K \frac{III_V - 1}{III_V}. \quad (8)$$

It can be seen that all of the experimental constants that were present in the original Ogden model are now absent. The expression  $f_0(\lambda_i)$  is defined in equation (9)

$$f_0(\lambda_i) = \sum_{x=0}^{\infty} \lambda_i^{\left(-\frac{1}{2}\right)^x} \cdot \sigma_0 \left( \lambda_i^{\left(-\frac{1}{2}\right)^x} - 1 \right). \quad (9)$$

The series in equation (9) calculate one value of  $f_0(\lambda_i)$  at a time, from the uniaxial data, by summing over  $x$  until a reasonable tolerance is met. At the beginning of the simulation, a sufficient number of  $f_0(\lambda_i)$  is found from equation (9) and corresponds to a particular value of  $\lambda_i$ . [5]

These values of  $f_0(\lambda_i)$  are obtained from the tabulated uniaxial experimental data. It is not required anymore to solve for experimental constants. It is expected that satisfactory results under any kind of loading can be obtained, hence not just for uniaxial loading. [5]

It is also possible to handle rate effects With **\*MAT\_183**. The material model permits the user to tabulate a table of uniaxial loading curves that each correspond to a particular strain rate, along with a single uniaxial unloading curve. If calculated loading rates differ from the tabulated loading curves, **\*MAT\_183** interpolates between the different loading curves. [5]

The total loading depends on strain and strain rate. Due to this dependence the unloading has to be determined through the use of a damage function. As described in Kolling [6], the damage function is unequal zero when unloading begins. The damage function  $d$  depends on the ratio of total deformation energy  $W$  to the maximum deformation energy  $W_{max}$ , see equation (10)

$$d = d \left( \frac{W}{W_{max}} \right). \quad (10)$$

The maximum deformation energy  $W_{max}$  is the energy that was generated during the loading history. According to equation (11) the damage function is then applied to the deviatoric part only

$$(\sigma_i)_{t'} = (1 - d) \left( (\sigma_i)_t - K \frac{III_V - 1}{III_V} \right) + K \frac{III_V - 1}{III_V}. \quad (11)$$

The expression  $(\sigma_i)_{t'}$  describes the stress, which occurs at a time  $t' = t + \Delta t$ . For more details on the development of this model reference is made to [6]. [5]

### 3 Simulation of tensile tests

In the next subchapters the general FE modelling, the general settings and the simulation results of the calculated tensile tests are elaborated.

#### 3.1 Modelling of tensile test

To get material data through tensile tests standardized specimens were used. For a comparison between test data and simulation results it is necessary to create an identical specimen in the simulation. The specimen has to be discretized with elements with a suitable size. Therefore, an analysis concerning the element size was done. The element size was minimized step by step until no change in the simulation results was registered. In Fig.1 the discretized tensile specimen is shown. As can be seen the specimen is fixed on the left side. The boundary conditions on the right side are fixed in y and z axes and in x direction a defined movement is given. Thus, the boundary conditions are defined according to the fixation in a real testing machine.

Constant stress solid elements are used, preferably shaped as hexahedrons. There is the possibility to change the element formulation from constant stress solid elements to e.g. fully integrated element formulation [7]. Through this setting hourglass modes do not occur, but the calculation is much more costly.

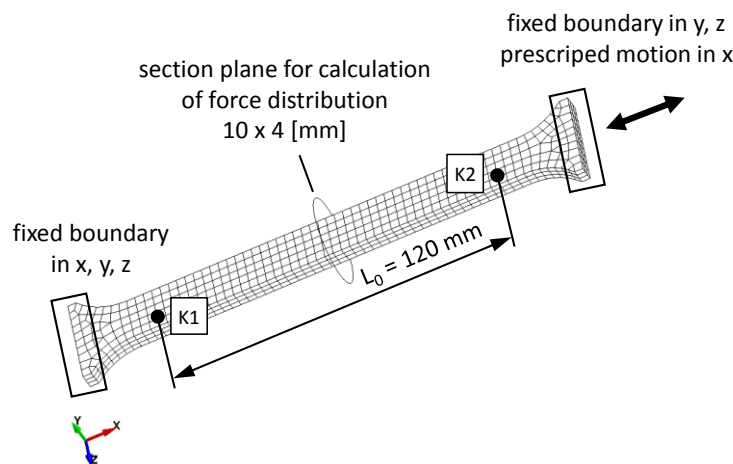


Fig.1: Discretized tensile specimen.

To enable a comparison between the simulation results and the test data the calculated forces  $F(t)$  and displacements  $L(t)$  have to be translated into stress  $\sigma$  and strain  $\varepsilon$ . The stress  $\sigma$  is calculated with equation (12)

$$\sigma = \frac{F(t)}{A_0} . \quad (12)$$

The variable displacement  $L(t)$  is translated to strain  $\varepsilon$  with equation (13)

$$\varepsilon = \frac{L_0 - L(t)}{L_0} = \frac{\Delta L(t)}{L_0} . \quad (13)$$

The force and displacement values  $F(t)$  and  $L(t)$ , respectively  $\Delta L(t)$ , are variable and create the non-linear curve progression in the stress-strain diagram. The subscription "0" describes values of the undeformed specimen.

The output data  $F(t)$  and  $\Delta L(t)$  have to be assigned in advance. To get a force distribution  $F(t)$  over the cross section  $A_0$  during loading the keyword `*DATABASE_CROSS_SECTION_PLANE_ID` is used. With this keyword the location and the orientation of the cross section  $A_0$  can be defined. In Fig.1 the section plane is shown. To enable the calculation of the strain  $\varepsilon$  the keyword `*DATABASE_HISTORY_NODE_ID` is used. In this card the nodes K1 and K2, see Fig.1, are selected. During post processing the difference between the x-displacement of the nodes K1 and K2 can be calculated which leads to  $\Delta L(t)$ . To get output data for the stress and strain calculations the keywords `*DATABASE_SECFORC` and `*DATABASE_NODOUT` are used. [7]

For the description of the material behaviour the material model `*MAT_183` is used, see chapter 2.1. Fig.2 shows the stress-strain diagram with the material characteristic data, which are read in through

the material card. As can be seen there are strain rate dependent values in the pressure case available, but not for the tensile case. The unloading curve belongs to the loading curve with the smallest rate.

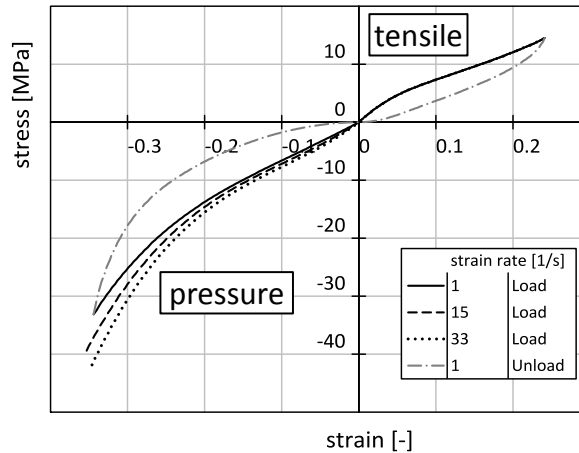


Fig.2: Material characteristic data for \*MAT\_183.

In Table 1 the available parameters in \*MAT\_183 are listed. The density  $ro$  was determined by weighting and measuring the volume of a real damper. To get the bulk modulus  $k$  a material test was done [4]. The parameters damping coefficient  $mu$ , shear modulus  $g$  and limit stress  $sigf$  are chosen according to previous calculations. The parameters  $sgl$ ,  $sw$  and  $st$  describe the dimensions of the specimen. It is possible to read in force and displacement values. The translation to the stress-strain relation will be done automatically due to the dimensions of the specimen. If there are stress and strain values from material tests available the parameters  $sgl$ ,  $sw$  and  $st$  have to be set to 1. The ID number under the designation  $lc/tbid$  defines the material data in the loading case. It is possible to enter a single curve or a tabulated strain rate dependent series of curves. In the considered case a table is defined.

The unloading response of \*MAT\_183 is controlled through the parameter  $tension$ . In the most realistic case ( $tension = 1$ ) rate effects are applied in all cases (loading, unloading, tension and compression). But this case is also the numerically most problematic one, because instabilities can occur. Therefore, two other formulations are available. On the one hand, rate effects in compression only ( $tension = 0$ ) and on the other hand rate effects in loading only ( $tension = -1$ ). In the simulation of the tensile test there is no difference by varying the parameter  $tension$ , because the material data in the tensile case are not rate dependent, see Fig.2. [8]

If material data for different strain rates are inserted ( $lc/tbid \triangleq$  table), the type has to be defined. On the one hand there is the possibility to choose true strain rate values ( $rtype = 0$ ) and on the other the engineering strain rate data ( $rtype = 1$ ). The material data, shown in Fig.2, are according to the engineering strain rate.

With the parameter  $avgopt$  the averaging option of rate depended calculations is chosen. If  $avgopt = 0$ , a 12 point simple average will be made. Through the setting of  $avgopt = 1$ , a 12 point running average is used [6]. This value is investigated in chapter 4.2.

Table 1: Selectable parameters in \*MAT\_183.

Designation	Value	Unit
$ro$	$1,179 \cdot 10^{-9}$	t/mm <sup>3</sup>
$k$	2700	MPa
$mu$	0,1	-
$g$	130	MPa
$sigf$	0	MPa
$sgl$	1	mm
$sw$	1	mm
$st$	1	mm
$lc/tbid$	table	-
$tension$	-1	-
$rtype$	1	-
$avgopt$	1	-

### 3.2 Simulation results of tensile tests

Fig.3 shows the simulation results of the tensile test in a stress-strain diagram. Also there is shown the load type in a displacement-time diagram. As can be seen, the diagram contains two calculation results (FEM). The difference between the two simulations is the strain rate caused by the different load periods of 0.01 s and 1.0 s. There are only small deviations between the two simulation results, because no rate dependent material data are available for tensile cases, see Fig.2. Also there is only a small difference between the test data and the calculated data.

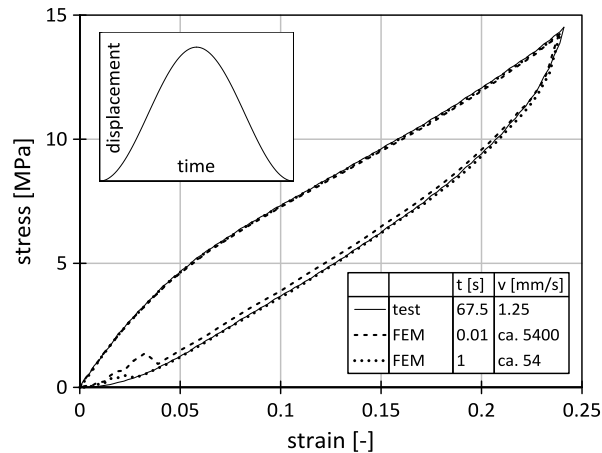


Fig.3: Comparison between material characteristic data (test) and simulation results (FEM).

## 4 Simulation of pressure test

Identically to the simulation of the tensile test, in the following subchapters the FE modelling, the general settings and the simulation results of calculated pressure tests are given. Because dampers in deep-drawing dies are loaded nearly completely in compression, there are additional investigations. These are a parameter analysis of the values that are contained in the **\*MAT\_183**, an investigation of the hysteresis behaviour and an investigation of repeated load cycles.

### 4.1 Modelling of the pressure test

The specimens of the pressure tests are small cylinders, which are cut out of real dampers. As for the tensile test, the specimen have to be created according to the true dimensions. This geometry is discretized with constant stress solid elements. Fig.4 illustrates the discretized pressure specimen on the left side. The shape has hexahedral form.

In contrast to the tensile test it is not possible to add the boundary conditions directly to the specimen. That is why it is necessary to include additional components to the simulation. These additional components are the fixed support and the moveable hydraulic jack, see Fig.4 on the right side. The support and the jack are considered as cylindrical rigid walls. That means that deformations are not possible. Also inertia effects are neglected. In both cases it is necessary to define node sets. The sets contain the nodes that are in interaction with the rigid walls. For these sets, the contact conditions are active. In the present case these are the upper and lower plane surfaces. Furthermore, it is necessary to define values for the location and the orientation. In the simulation of the pressure test the location and the orientation are given by the specimen's location and orientation at the beginning of the simulation. In a final step the simulation needs geometrical data for the rigid wall. [7]

Once again, to calculate stresses and strains in the postprocessor, a translation of force and displacement values is needed, see equations (12) and (13). For the output of force data  $F(t)$  again a cross section plane is applied, see Fig.4. The keyword for outputs is **\*DATABASE\_SECFORC**, see chapter 3.1. The strain  $\Delta L(t)$  is calculated due to the displacement of a node, that belongs to the upper plane surface. With the keywords **\*SET\_NODE\_LIST\_TITLE** and **\*DATABASE\_NODOUT** the number of the node and the output of the displacement are defined. [7]

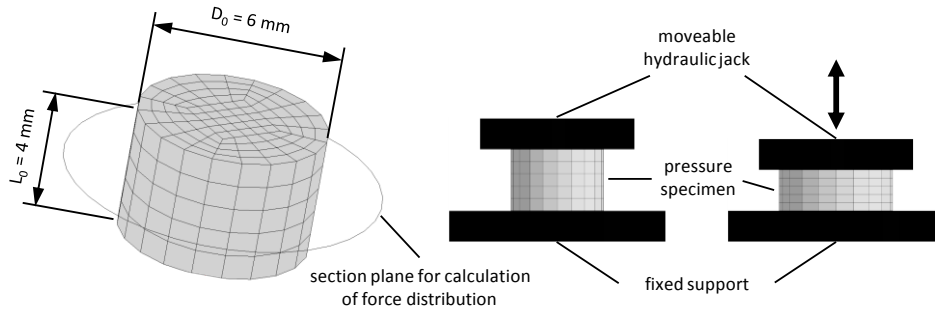


Fig.4: Discretized pressure specimen and additional components.

#### 4.2 Parameter analysis

To investigate the influence of the parameters in **\*MAT\_183** a parameter analysis is carried out. Table 2 shows the parameters with the varied values.

Table 2: Varied parameters in **\*MAT\_183**.

Designation	Description	Value	Unit
<i>mu</i>	damping coefficient	0,00 0,01 0,50	-
<i>g</i>	shear modulus	0 50 130	MPa
<i>sigf</i>	limit stress	0,0 0,1 0,5 1,0	MPa
<i>tension</i>	parameter that controls how the rate effects are treated	-1 0 1	-
<i>avgopt</i>	averaging option for strain rate treatment	0 1	-

Fig.5 depicts the simulation results by varying the damping coefficient *mu*. If the value of *mu* is small, e.g.  $mu \leq 0.1$ , there are nearly no changes in the simulation results. By further increasing of *mu* the calculation becomes instable and oscillations occur, see the enlarged view in Fig.5 on the right side. The curve with  $mu = 0.01$  seems to be realistic. So this value is retained for further simulations.

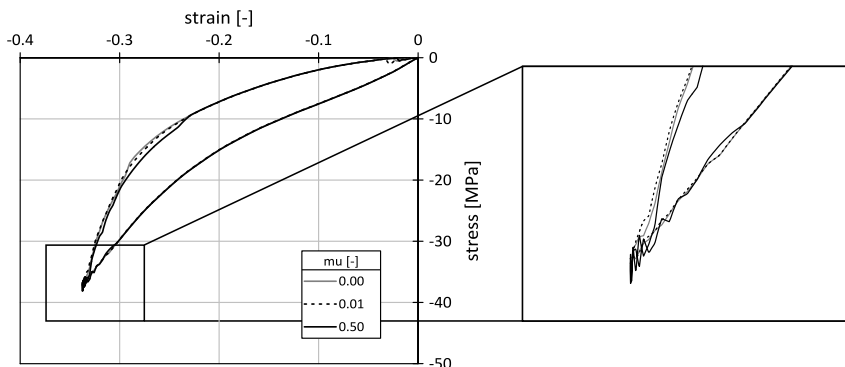


Fig.5: Simulation results by varying the damping coefficient *mu*.

The shear modulus *g* and the limit stress *sigf* for frequency independent damping are linked. They define a perfectly plastic model that runs in parallel to the hyperelastic model and simulates internal friction in the rubber. Hence the simulation of irreversible deformations is possible. If the shear modulus is set  $g = 0$  the parallel running model is deactivated and no deformation remains [9]. In the following, the

influence of these two parameters is investigated. In the first simulation series the shear modulus  $g$  is varied and the limit stress  $sigf$  is set constant. In Fig.6 the results are shown. In every simulation the general curve progression is the same. But in the area of the point of origin there are deviations. As can be seen in the enlarged view in Fig.6 the higher the shear modulus the lower the irreversible deformation. As mentioned before, if the shear modulus is set to  $g = 0$  no deformation remains. So the curve of this calculation begins and ends in the point of origin.

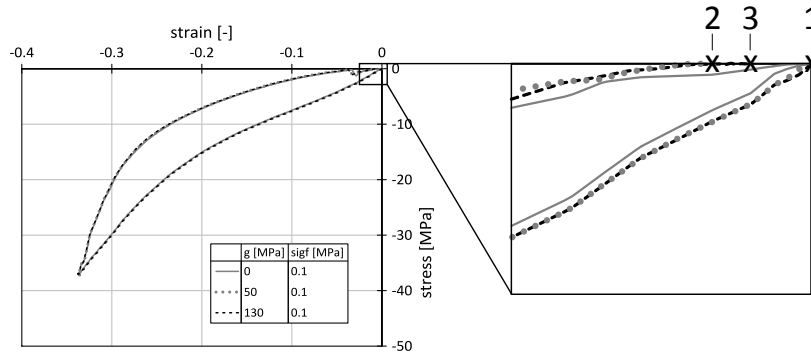


Fig.6: Simulation results by varying the shear modulus  $g$  and constant limit stress  $sigf$ .

In Table 3 the results regarding the irreversible deformation by varying the shear modulus  $g$  are summarized. The data relate to the initial length  $L_0 = 4$  mm of the pressure specimen. Thus, it seems that the irreversible deformation increases by decreasing shear modulus  $g$ .

Table 3: Irreversible deformations relate to the initial length of the pressure specimen by varying the shear modulus  $g$ .

Nr. acc. Fig.6	$g$ [MPa]	$sigf$ [MPa]	irreversible deformation [mm]	irreversible deformation [%]
1	0	0,1	0,00	0,00
2	50	0,1	0,02	0,48
3	130	0,1	0,01	0,35

Fig.7 shows the simulation results by varying the limit stress  $sigf$  and constant selected shear modulus  $g$ . As can be seen in the enlarged view on the right side the higher the limit stress  $sigf$  the higher the irreversible deformation. Furthermore, a secondary effect appears. If the limit stress  $sigf$  increases also the stiffness at the beginning of the loading cycle increases.

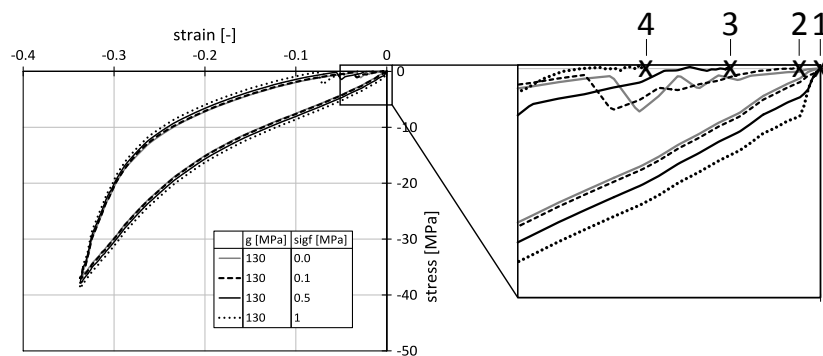


Fig.7: Simulation results by varying the limit stress  $sigf$  and constant shear modulus  $g$ .

In Table 4 the irreversible deformation are listed. Once again, the data relate to the initial length  $L_0 = 4$  mm of the pressure specimen. As demonstrated in the table by increasing the limit stress  $sigf$  also the irreversible deformation increases.

Table 4: Irreversible deformations relate to the initial length of the pressure specimen by varying the limit stress  $\text{sigf}$ .

Nr. acc. Fig.7	$g$ [MPa]	$\text{sigf}$ [MPa]	irreversible deformation [mm]	irreversible deformation [%]
1	130	0,0	0,00	0,00
2	130	0,1	0,01	0,35
3	130	0,5	0,05	1,47
4	130	1,0	0,11	2,75

In the next step the parameter  $\text{tension}$  is analysed. This parameter controls how the rate effects are treated. It has only an effect if a table for rate effects is defined under  $\text{lc/tbid}$ . For more information see chapter 3.1. Fig.8 shows the simulation results. In the loading case nearly identical results appear. In the unloading case there are also nearly the same curves for  $\text{tension} = 0$  and  $\text{tension} = 1$ . That makes sense due to the fact that this two settings are responsible for rate effects in the pressure case for loading and unloading. If this parameter is set to  $\text{tension} = -1$  no rate effects in unloading are considered. So the resistance against the deformation becomes smaller and the calculated unloading curve is closer to the abscissa. To illustrate the high strain rate, which was used in these calculations, Fig.8 additionally contains the experimental material characteristic data.

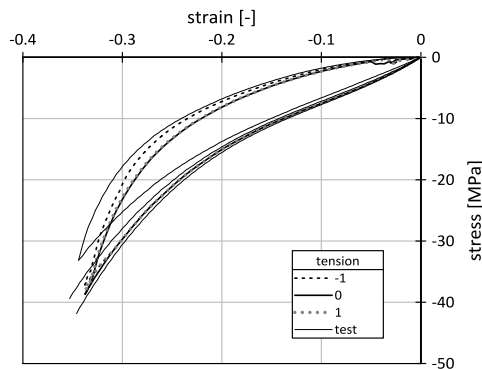


Fig.8: Simulation results by varying the parameter  $\text{tension}$ .

Fig.9 shows the simulation results by varying the parameter  $\text{avgopt}$ . If a table is defined under  $\text{lc/tbid}$ , this parameter is responsible for the averaging option by determining the strain rate. For more information see chapter 3.1. As can be seen in Fig.9 the results are non-satisfying if  $\text{avgopt} = 0$ . If the parameter is set to  $\text{avgopt} = 1$  the curve characteristic is much smoother. That results from the special smoothing strategy in the case of reversal from loading to unloading [6].

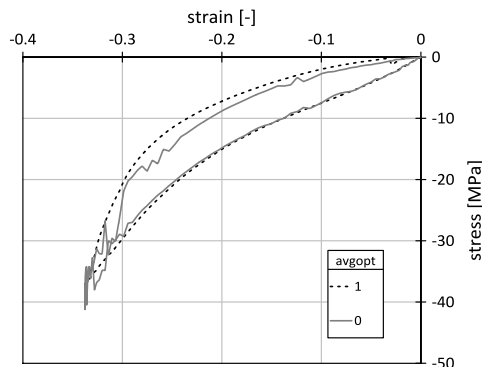


Fig.9: Simulation results by varying the parameter  $\text{avgopt}$ .

### 4.3 Hysteresis

A further investigation gives attention to the hysteresis behaviour. An additional material test was done. A pressure specimen was loaded with different displacements. The force and displacement data was translated to stress and strain data, identically to the tests for material characteristic data, which are



used in the material card **\*MAT\_183**. To enable the comparison between test data and simulation results the loading displacements in LS-DYNA have to be modified. That means that different calculations with different height of defined displacements of the virtual hydraulic jack (rigid wall) have to be done. Fig.10 shows the compared results. In the loading cases the curves of tests and simulations are nearly the same. In the unloading cases there are acceptable deviations. The small deviations can be explained by the load type in the testing machine. The load type was programmed linear and at every reversal point from loading to unloading there was a hold point. As a result, the material of the specimen relaxed [3]. The material model **\*MAT\_183** doesn't offer the consideration of relaxation. But LS-DYNA contains several other material models, which are able to consider the relaxation, e.g. **\*MAT\_127**. If relaxation should be considered by using **\*MAT\_183**, the unloading curve can be modified. However, in this case the material data fits only to one time interval of the hold point.

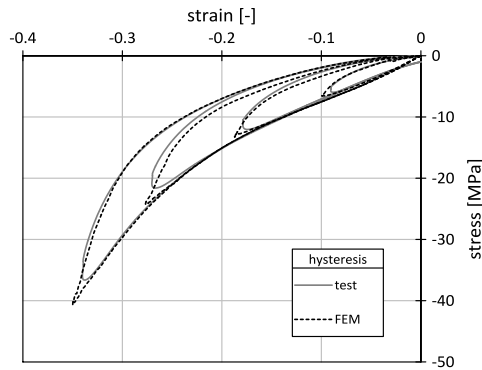


Fig.10: Comparison between material characteristic data (test) and simulation results (FEM) referring to the hysteresis behaviour.

#### 4.4 Repeated loading

In technical processes repeated loading often occurs. In deep-drawing dies huge masses are accelerated and stopped quickly. To prevent oscillations, dampers are used, which are charged and discharged permanently. Thus, it is necessary to simulate repeated loading cases. Fig.11 illustrates the simulation results of a repeated loading. A pressure specimen is compressed two times. The strongly oscillating curve characteristic of the second load cycle is clearly visible. The reason for this behaviour are numerical instabilities [9]. Consequently, simulations of repeated loads are not possible by using **\*MAT\_183**. Furthermore, as can be seen in Fig.11, the curve of the second load cycle follows the unloading curve, because the unloading is implemented in **\*MAT\_183** as a damage function. Consequently the reloading follows the unloading path [9]. Unfortunately, that is not realistic.

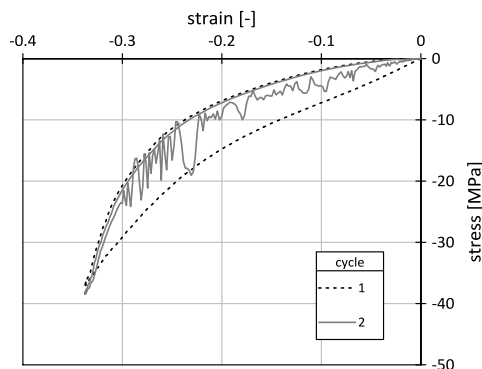


Fig.11: Simulation results in a repeated loading case.

#### 5 Simulation of a real damper

A final investigation considers the simulation of a damper [1] as used in deep-drawing dies, see Fig.12. The damper has a tubular shape. The cross section was measured with a contact measurement device, which is a source for a deviation in shape, especially in the inner region, see below. Subsequently the cross section was rotated around an axis to obtain a volumetric body. In the following the modelling and the results are described.

## 5.1 Modelling

The modelling of a real damper is similar to the modelling of the pressure test. The material tests with the damper also were made in a similar testing machine. Therefore, a support and a hydraulic jack have to be implemented in the simulation. These components are simplified by rigid walls. The components of the simulation are shown in Fig.12. In the case of damper tests additional cylindrical walls in the middle of the damper elements are included. Supports like this were also used in the material tests. The general settings, such as element formulation, parameters in `*MAT_183`, etc. are transferred from the simulation of the pressure tests. Only the use of the keyword `*CONTACT_AUTOMATIC_SINGLE_SURFACE_ID` [7] differs to the pressure test calculations. This keyword is needed if the damper's surfaces come in contact with itself.

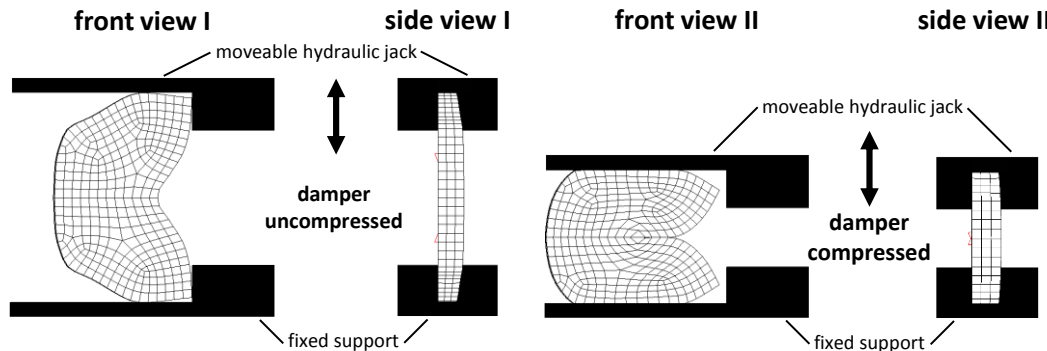


Fig.12: Tubular damper [1] with additional components for the simulation.

Fig.12 shows that only a small section of the whole damper is discretized. Through the definition of additional coordinate systems and boundary conditions at the planar surfaces it is possible to use the damper's symmetry. The movement rectangular to the planar surface axis has to be locked. Along the other two axes the movements have to be free.

## 5.2 Results and discussions

In Fig.13 the material test data are compared to the simulation results. As can be seen the characteristic of the curve progression is similar.

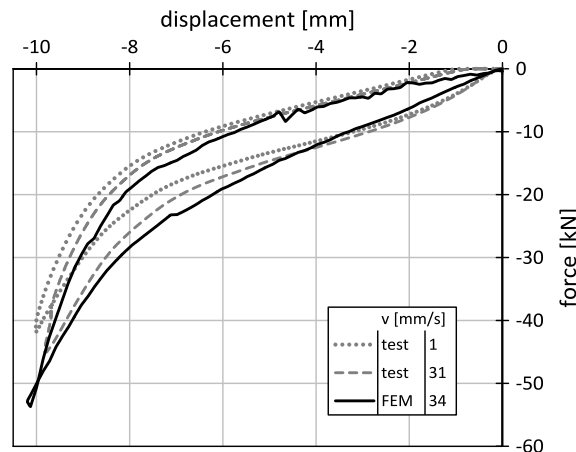


Fig.13: Comparison between material test data (test) and simulation results (FEM).

As mentioned before there is the possibility that the measured cross section is not exactly the same as the true one. Furthermore, the measured damper is not identical to the damper from the material tests. To illustrate the influence of the damper shape the cross section was modified. In Fig.13 the simulation results of this comparison are shown. The shape of damper 1 corresponds to a used one. The second damper corresponds to a new damper. The diagram shows the counteracting forces. The used damper reacts with a higher resistance against the deformation. Due to irreversible deformation its cross section shape became smaller in height and taller in width. At constant defined displacement  $s = 10.2$  mm the tubular damper provides more material for resistance against the deformation.

As another characteristic in Fig.13 the rate dependence is shown. In both cases, shapes of damper 1 and damper 2, the stiffness of the rubber is higher at higher velocity  $v$ .

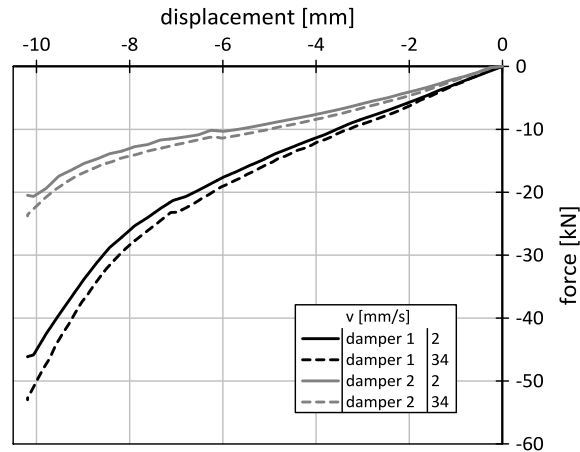


Fig. 14: Simulation results at various damper shapes.

## 6 Conclusions

Material tests for tensile and pressure loading have been done in advance. These tests provided material characteristic data, which was used in LS-DYNA. For validation purposes the two material tests were simulated by using the material model **\*MAT\_183**.

The curve progression in the stress-strain diagram of the tensile and pressure test simulations are nearly identical to the experimental material data. Furthermore, it is possible to consider the strain rate dependency with **\*MAT\_183** if material characteristic data are available. Also a material damage (irreversible deformation) and hysteresis behaviour can be considered. One disadvantage of **\*MAT\_183** is the numerical instability in repeated loading cases (reloading after unloading) [9]. In repeated loading cases the reloading follows the unloading path [9]. That describes a non-physical behaviour and has a disadvantageous effect for simulations of rubber parts in deep-drawing dies.

The obtained material data and understanding of the behaviour of **\*MAT\_183** were applied to simulate a damper, which is used in deep-drawing dies. Also for these simulations material test data were available for comparison to the simulation results. The curve progressions of test data and simulation results in the force-displacement diagram are in good agreement.

## 7 Future work

The friction between damper and further components (support, hydraulic jack) should be considered. Hence, e.g. solid elements instead of rigid walls have to be used for the additional parts. Alternatively to **\*MAT\_183** the material model **\*MAT\_181** can be used to consider repeated loading cycles [9]. Furthermore, a study concerning damage (irreversible deformation) can be carried out. Also an additional material test with a damper should be made. The damper's shape has to be measured before and after the test. Simulations with the corresponding damper shapes have to be carried out. Finally the test data and the simulation results can be compared more realistically.

## 8 References

- [1] MöllerMiner GmbH. <http://www.moellergroup.com/>.
- [2] LSTC Inc. LS-DYNA (a general-purpose finite element program).
- [3] Stommel, M., Korte, W., and Stojek, M. 2011. *FEM zur Berechnung von Kunststoff- und Elastomerbauteilen*. Hanser, Carl, München.
- [4] Austrell, P.-E. 1997. *Modeling of elasticity and damping for filled elastomers*. Report, Lund University.
- [5] Freidenberg, A., Lee, C. W., Durant, B., Nesterenko, V. F., Stewart, L. K., and Hegemier, G. A. 2013. Characterization of the Blast Simulator elastomer material using a pseudo-elastic rubber model. *International Journal of Impact Engineering* 60, 58–66.
- [6] Kolling, S., Du Bois, P. A., Benson, D. J., and Feng, W. W. 2007. A tabulated formulation of hyperelasticity with rate effects and damage. *Comput Mech* 40, 5, 885–899.
- [7] LS-Dyna. 2014. *Volume I. Keyword Users's Manual*.
- [8] Benson, D. J., Kolling, S., and Du Bois, Paul A. 2013. A Simplified Approach for Strain-Rate Dependent Hyperelastic Materials with Damage.
- [9] Du Bois, P. A. 2014/2015, personal communication.